ELSEVIER

Physics of the Earth and Planetary Interiors 128 (2001) 25–34

PHYSICS OF THE EARTH AND PLANETARY INTERIORS

www.elsevier.com/locate/pepi

# A numerical dynamo benchmark

U.R. Christensen [a,*], J. Aubert [b], P. Cardin [b], E. Dormy [c], S. Gibbons [d], G.A. Glatzmaier [e], E. Grote [f], Y. Honkura [g], C. Jones [d], M. Kono [h], M. Matsushima [g], A. Sakuraba [i], F. Takahashi [g], A. Tilgner [f], J. Wicht [a], K. Zhang [d]

[a] *Institut für Geophysik, Universität Göttingen, Herzberger Landstrasse 180, 37075 Göttingen, Germany*
[b] *LGIT, Observatoire des Sciences de l'Univers de Grenoble, B.P. 53, 38041 Grenoble Cedex 09, France*
[c] *Institut de Physique du Globe de Paris, 4 Place Jussieu, 75252 Paris Cedex 05, France*
[d] *Department of Mathematics, University of Exeter, Exeter EX4 4QE, UK*
[e] *Earth Sciences Department, University of California, Santa Cruz, CA 95064, USA*
[f] *Theoretische Physik IV, Universität Bayreuth, 95440 Bayreuth, Germany*
[g] *Department of Earth and Planetary Sciences, Tokyo Institute of Technology, 2-12-1 Ookayama, Meguro-ku, Tokyo 152-8551, Japan*
[h] *Institute for Study of the Earth's Interior, Okayama University, Yamada 827, Misasa, Tottori-ken 682-0193, Japan*
[i] *Department of Earth and Planetary Physics, University of Tokyo, Hongo 7-3-1, Bunkyo-ku, Tokyo 113-0033, Japan*

Received 31 December 2000; accepted 14 August 2001

**Abstract**

We present the results of a benchmark study for a convection-driven magnetohydrodynamic dynamo problem in a rotating spherical shell. The solutions are stationary aside from azimuthal drift. One case of non-magnetic convection and two dynamos that differ in the assumptions concerning the inner core are studied. Six groups contributed numerical solutions which show good agreement. This provides an accurate reference standard with high confidence. © 2001 Elsevier Science B.V. All rights reserved.

*Keywords:* Geodynamo; Numerical modeling

## 1. Introduction

In recent years, three-dimensional simulations of convection-driven magnetohydrodynamic dynamos in rotating spherical shells have become possible and are progressively employed to develop an understanding for the origin of the Earth's magnetic field and its spatial and temporal structure. The first models employed hyperdiffusivities and either neglected inertia or included only the axisymmetric part (Glatzmaier and Roberts, 1995; Kuang and Bloxham, 1997) or they assumed somewhat artificial boundary conditions for the magnetic field Kageyama and Sato (1995). Later models with more moderate values of the control parameters did not use these approximations (for example, Christensen et al., 1998; Busse et al., 1998; Christensen et al., 1999; Katayama et al., 1999; Grote et al., 2000). Several numerical codes for dynamo modelling have been developed independently by various groups, although they usually follow similar principles. The velocity and magnetic fields are represented by poloidal and toroidal scalar potentials and all the unknowns are expanded in spherical harmonic functions in the angular coordinates. Diffusive

* Corresponding author. Tel.: +49-551-39-7451; fax: +49-551-39-7459.
*E-mail address:* urc@uni-geophys.gwdg.de (U.R. Christensen).

0031-9201/01/$ – see front matter 
PII: S0031-9201(01)00275-8

terms in the equations are treated implicitly during time-stepping, while the non-linear terms are evaluated on grid points, which requires transformations between spectral and grid space (spectral transform method). The codes differ mainly in their treatment of the radial dependence and in the way the arising boundary value problems for each harmonic mode are solved. Some expand the variables in Chebyshev polynomials and use collocation methods, while others use finite differencing and grid representation. An exception is the method by Kageyama and Sato (1995), who have used finite differences throughout. Other codes that employ only local representations of the variables, for example by finite elements, are currently under development.

The verification of newly developed codes for complex nonlinear problems is not a simple task. Rigorous testing with analytical solutions is not possible for the fully non-linear problem. Comparison with other published solutions is difficult because they usually show chaotic time-dependence and because they make specific assumptions (for example, on boundary conditions or neglected terms), which are not implemented in other codes. The concept of a benchmark is to set up a simple, well defined and easily reproduced standard solution, which is confirmed by several independent codes and which is converged to great accuracy. It serves several purposes: (i) to increase the confidence in the correctness of the codes that contribute to the benchmark, (ii) to assess the accuracy and possibly the run-time performance of existing methods, and (iii) to assist future code developments by providing a well-established standard solution for verification.

The present benchmark was proposed at the study of the Earth's deep interior (SEDI) meeting of 1998 in Tours and has been expanded and modified as a result of discussions among the participants. Its basis is one of the few quasi-stationary dynamo solutions that have been reported in the literature (Christensen et al., 1999). The stationarity allows the comparison of well-defined numbers. Parameter values are moderate, so that high resolution is not required to reproduce the dynamo. The full inertia term is kept in the momentum equation and the concept of hyperdiffusivity is not used. In addition to the originally proposed dynamo with an insulating inner core co-rotating with the outer boundary (case 1), the cases of rotating non-magnetic convection (case 0) and that of a dynamo with a conducting and freely rotating inner core (case 2) have been added. Aside from global properties, such as kinetic and magnetic energies, where small inaccuracies may average out, some local values of the solution are also reported.

## 2. Definition of the benchmark cases

Thermal convection and magnetic field generation in a rotating spherical shell filled with an electrically conducting fluid are considered. The ratio of inner radius $r_i$ to outer radius $r_o$ is set to 0.35. Temperature is fixed to $T_o$ and $T_o + \Delta T$ on the outer and inner boundaries, respectively. The Boussinesq approximation is used and gravity varies linearly with radius. The equations are scaled with $D = r_o - r_i$ as the fundamental length scale, which makes the dimensionless radii equal to $r_o = 20/13$ and $r_i = 7/13$. The time scale is $D^2/\nu$, with $\nu$ the kinematic viscosity, $\nu/D$ is the scale for velocity $\boldsymbol{u}$, and $\Delta T$ for temperature $T$. The scaled temperature on the outer boundary is zero. Magnetic induction $\boldsymbol{B}$ is scaled by $(\rho\mu\eta\Omega)^{1/2}$, where $\rho$ is the density, $\mu$ the magnetic permeability, $\eta$ the magnetic diffusivity, and $\Omega$ is the basic rotation rate about the $z$-axis. The non-hydrostatic pressure $P$ is scaled by $\rho\nu\Omega$. The scaled equations are

$$E\left(\frac{\partial \boldsymbol{u}}{\partial t} + \boldsymbol{u}\cdot\nabla\boldsymbol{u} - \nabla^2\boldsymbol{u}\right) + 2\hat{z}\times\boldsymbol{u} + \nabla P = Ra\frac{\boldsymbol{r}}{r_o}T + \frac{1}{Pm}(\nabla\times\boldsymbol{B})\times\boldsymbol{B} \quad (1)$$

$$\frac{\partial \boldsymbol{B}}{\partial t} = \nabla\times(\boldsymbol{u}\times\boldsymbol{B}) + \frac{1}{Pm}\nabla^2\boldsymbol{B} \quad (2)$$

$$\frac{\partial T}{\partial t} + \boldsymbol{u}\cdot\nabla T = \frac{1}{Pr}\nabla^2 T \quad (3)$$

$$\nabla\cdot\boldsymbol{u} = 0, \quad \nabla\cdot\boldsymbol{B} = 0 \quad (4)$$

Non-dimensional control parameters are the modified Rayleigh number

$$Ra = \frac{\alpha g_o \Delta T\, D}{\nu\Omega} \quad (5)$$

where $\alpha$ is the thermal expansion coefficient and $g_o$ gravity at the outer radius, the Ekman

number

$$E = \frac{\nu}{\Omega D^2}, \tag{6}$$

the Prandtl number

$$Pr = \frac{\nu}{\kappa}, \tag{7}$$

where $\kappa$ is thermal diffusivity, and the magnetic Prandtl number

$$Pm = \frac{\nu}{\eta}. \tag{8}$$

The velocity vanishes on the rigid boundaries, relative to the state of rotation of the respective boundary. In cases 0 and 1, the inner and outer boundaries co-rotate. In case 1, the regions outside the fluid shell are electrical insulators and the magnetic field on the boundaries matches with appropriate potential fields in the exterior that imply no external sources of the field.

In case 2, the inner core is treated as an electrically conducting rigid sphere that can rotate around the $z$-axis relative to the outer boundary, which provides the frame of reference. Its moment of inertia is determined assuming the same density as in the liquid shell, and its angular acceleration results from viscous and magnetic torques. The moment of inertia is irrelevant for the final uniform rotation of the inner core, but influences the transient spinup. In the inner core Eq. (2) applies with the velocity field of rigid-body rotation and the same magnetic Prandtl number, i.e. the same electrical conductivity and magnetic permeability as in the fluid shell. At the boundary between inner core and fluid shell the magnetic field and the horizontal component of the electrical field are continuous.

The Ekman number is $E = 10^{-3}$ and the Prandtl number is $Pr = 1$ in all cases. In cases 0 and 1, we set the Rayleigh number to $Ra = 100$. In case 2, it is $Ra = 110$, which is approximately two times supercritical. The magnetic Prandtl number is zero in case 0 (non-magnetic convection) and is $Pm = 5$ in cases 1 and 2.

Because only the final quasi-stationary solutions are compared, the initial condition is, strictly speaking, not part of the benchmark definition. However, because non-magnetic convection is found stable against small magnetic perturbations at these parameters and because the dynamo solutions seem to have only a small basin of attraction, the initial state is of some concern. Also the existence of multiple dynamo solutions, for example with different azimuthal symmetry, cannot be ruled out. Here, we recommend a set of initial conditions, but any other conditions that lead to the desired solutions are also permissible. In all cases the initial velocity is zero and the initial temperature is

$$T = \frac{r_o r_i}{r} - r_i + \frac{210A}{\sqrt{17920\pi}} \times (1 - 3x^2 + 3x^4 - x^6)\sin^4\theta\cos 4\phi \tag{9}$$

where $\theta$ is the colatitude, $\phi$ the longitude, and $x = 2r - r_i - r_o$. This describes a conductive state with a perturbation of harmonic degree and order four superimposed. The amplitude is set to $A = 0.1$. In case 1, the initial magnetic field is for $r_i \le r \le r_o$:

$$B_r = \frac{5}{8}\left(8r_o - 6r - 2\frac{r_i^4}{r^3}\right)\cos\theta \tag{10}$$

$$B_\theta = \frac{5}{8}\left(9r - 8r_o - \frac{r_i^4}{r^3}\right)\sin\theta \tag{11}$$

$$B_\phi = 5\sin(\pi(r - r_i))\sin 2\theta. \tag{12}$$

This corresponds to a dipolar poloidal field created by a current density in the $\phi$-direction which is uniform in radius and a superimposed toroidal field of harmonic degree two. The maximum value of both $B_r$ and $B_\phi$ is 5. In case 2, the initial magnetic field is for $0 \le r \le r_o$:

$$B_r = 5\frac{4r_o - 3r}{3 + r_o}\cos\theta \tag{13}$$

$$B_\theta = 5\frac{9r - 8r_o}{2r_o + 6}\sin\theta \tag{14}$$

$$B_\phi = 5\sin\left(\pi\frac{r}{r_o}\right)\sin 2\theta. \tag{15}$$

## 3. Character of the solution

Starting from the recommended initial condition, a quasi-stationary solution is reached within approximately 15 time units in cases 1 and 2 and within 1.2 time units in case 0. The solution can be expressed by a vector function of the form

$$(\boldsymbol{u}, \boldsymbol{B}, T) = \boldsymbol{f}(r, \theta, \phi - \omega t) \tag{16}$$

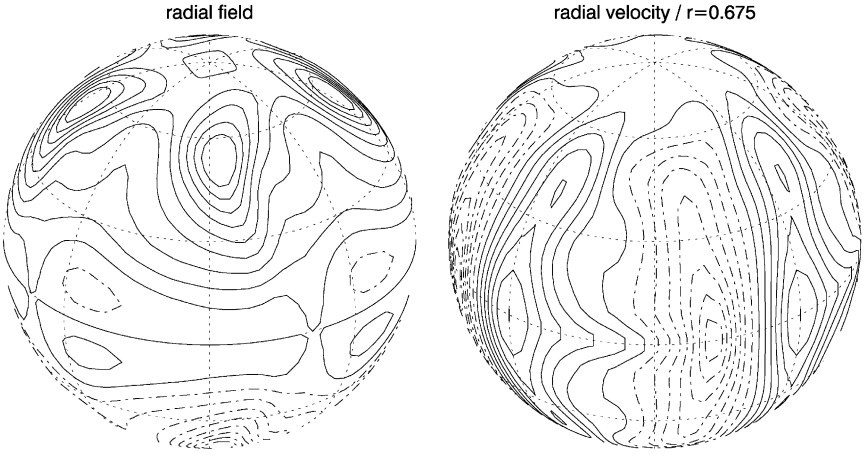


Fig. 1. Case 1: left, contours of $B_r$ on outer boundary in steps of 0.25; right, contours of $u_r$ at mid-depth in the shell, interval 2. Positive and zero contours solid lines, negative contours dash-dotted.

with $\omega$ being the drift frequency. In case 2, the inner core rotates at a uniform rate $\omega_{\rm ic}$ with respect to the outer boundary after the initial transient. The solutions are symmetric about the equator (dipole parity) and have fourfold symmetry in longitude. In order to reduce computer time, in some calculations this symmetry has been exploited by restricting the spherical harmonic expansions accordingly. This is safe because tests show that the solution is stable against small symmetry-breaking perturbations. Some aspects of the solution for case 1 are visualised in Fig. 1. Convection is columnar and the magnetic field on the outer boundary is strongly dipolar and dominated by four flux lobes. The figure shows a result obtained with moderate resolution and is meant for illustrative purposes only. The presence of a conducting and rotating inner core in case 2 has no strong effect of the overall pattern of the solution.

## 4. Requested data

Global averages as well as local data at a specific point are compared in this benchmark. In all cases, the drift frequency $\omega$ and the mean kinetic energy density in the fluid have been calculated as

$$E_{\rm kin} = \frac{1}{2V_{\rm s}} \int_{V_{\rm s}} \boldsymbol{u}^2 \, {\rm d}V \tag{17}$$

where $V_{\rm s}$ refers to the volume of the fluid shell. In cases 1 and 2, the mean magnetic energy density in the shell is calculated as

$$E_{\rm mag} = \frac{1}{2V_{\rm s}EPm} \int_{V_{\rm s}} \boldsymbol{B}^2 \, {\rm d}V. \tag{18}$$

In case 2, also the magnetic energy density $E^{\rm ic}_{\rm mag}$ in the inner core, defined equivalently to Eq. (18) for the inner core volume $V_{\rm ic}$, and the angular frequency $\omega_{\rm ic}$ of differential rotation of the inner core are requested. When participants compared preliminary results in the course of the benchmark study, the torque acting on the inner core turned out to be useful to identify errors. Therefore we also list the values of the Lorentz torque $\Gamma_{\rm L}$ scaled by $\rho D \nu^2$.

Defining a point where local data are to be taken is not trivial because it must be fixed in the drifting frame of reference. We take a point at mid-depth ($r = (r_{\rm i} + r_{\rm o})/2$) in the equatorial plane ($\theta = \pi/2$) whose $\phi$-coordinate is given by the conditions $u_r = 0$ and $(\partial u_r/\partial\phi) > 0$. For this point we request in cases 0 and 1 the values of $T$ and $u_\phi$ and additionally in case 1 the value of $B_\theta$.

## 5. Methods

Six groups have contributed results to some or all of the benchmark cases. Here, each code is described briefly by some keywords. A more complete description can be found in the supplied references.

*Aubert, Cardin and Dormy (ACD)*: Spherical harmonic expansion, finite differences in the radial direction (Dormy et al., 1998). The radial mesh interval decreases in geometrical progression towards the boundaries. Three-point stencil for second-order derivatives and five-point stencil for biharmonic operators (second-order accurate). Symmetry in longitude can be imposed.

*Christensen, Wicht and Glatzmaier (CWG)*: Spherical harmonic expansion, Chebyshev polynomials in radial direction, alias-free transform (Glatzmaier, 1984; Christensen et al., 1999); the basic numerical method was also used in (Glatzmaier and Roberts, 1995). Symmetry in longitude assumed in most cases. Time step dynamically controlled, typically $1.5 \times 10^{-4}$ at low spatial resolution and $0.75 \times 10^{-4}$ at high resolution. Different versions of this code have been run on the benchmark problems by Christensen and Wicht and by Glatzmaier, respectively. Results obtained by Glatzmaier are marked by an asterisk (*).

*Gibbons, Jones and Zhang (GJZ)*: Spherical harmonic expansion, finite-differencing in radial direction with non-equidistant grid using the Chebyshev zeros as grid points and a seven-point stencil for all derivatives.

*Kono and Sakuraba (KS)*: Spherical harmonic expansion, Chebyshev tau method (Canuto et al., 1987) for radial coordinate (Sakuraba and Kono, 1999).

*Tilgner and Grote (TG)*: Spherical harmonic expansion, Chebyshev polynomials in radial direction (Busse et al., 1998; Tilgner, 1999).

*Takahashi, Matsushima and Honkura (TMH)*: Spherical harmonic expansion, finite difference with option for equidistant or non-uniform grid (Chebyshev points) in radial direction. Pressure defined on staggered grid points. Three-point stencil used for second-order derivatives and four-point stencil for derivatives at staggered grid points. Longitudinal symmetry exploited.

The three codes which use an expansion in Chebyshev polynomials in the radial direction (CWG, KS and TG) are structured very similarly. The three codes using finite differences in the radial direction (ACD, GJZ and TMH) differ for example in the order of the difference scheme and the structuring of the radial grid.

Most groups provide results at different resolution. All use 8-byte words (double precision). The spherical harmonic expansion is truncated at degree $\ell_{\max}$ and order $m_{\max}$. Most contributors include all terms with harmonic order $m \leq \ell \leq \ell_{\max}$ ($m_{\max} = \ell_{\max}$, triangular truncation), except GJZ, who truncate in most cases at $m \leq \min(\ell, m_{\max})$ with $m_{\max} < \ell_{\max}$ (trapezoidal truncation). The minimum necessary number of grid points in $\theta$-direction (Gauss points), on which non-linear products are calculated, is $\ell_{\max} + 1$, but some authors use a larger number of points $N_\theta$ to reduce aliasing effects (similarly in $\phi$-direction). For alias-free computations of the non-linear terms $N_\theta$ needs to be equal or greater than $(3\ell_{\max} + 1)/2$ and for triangular truncation of the spherical harmonics the number of grid points in longitude needs to be twice this. In those codes which use a spectral representation in the radial direction, the number of radial grid points $N_r$ may exceed the number of Chebyshev modes $N_c$, although in the present cases $N_r \simeq N_c$ has been used.

## 6. Results

At a qualitative level, all contributors obtain the same generic solutions, which is the prerequisite for a quantitative comparison and a convergence test. In order to compare specific numbers obtained with different codes at different resolution and in order to monitor convergence, we define as resolution $R$ the third root of the number of degrees of freedom for each scalar variable:

$$R = N_r^{1/3}(\ell_{\max}[2m_{\max} + 1] - m_{\max}^2 + m_{\max} + 1)^{1/3}. \tag{19}$$

For $m_{\max} = \ell_{\max}$ this reduces to $R = N_r^{1/3}(\ell_{\max} + 1)^{2/3}$. In case 2, $N_r$ refers to the combined number of radial points in the fluid shell and in the inner core.

### 6.1. Non-magnetic convection (case 0)

All results for case 0 are listed in Table 1. In Fig. 2, we compare most of the results as functions of $R$. Note that for each quantity except $\omega$ the range in the diagram is less than 2% of the absolute value. That is, all results that fall into the diagram agree within better than 2%. All results seem to converge towards the same point. The convergence is clearest for the fully spectral code by CWG (circles), where results at comparatively low resolution differ only marginally from those with high

Table 1
Results for benchmark case 0[a]

| Group | $N_r$ | $N_\theta$ | $\ell_{max}$ | $E_{kin}$ | $T$ | $u_\phi$ | $\omega$ |
|---|---|---|---|---|---|---|---|
| ACD | 50 | 46 | 44 | 58.970 | 0.4259 | −10.058 | 0.0602 |
| ACD | 100 | 46 | 44 | 58.515 | 0.4276 | −10.134 | 0.1509 |
| ACD | 150 | 46 | 44 | 58.426 | 0.4279 | −10.147 | 0.1686 |
| ACD | 250 | 92 | 44 | 58.379 | 0.4280 | −10.153 | 0.1775 |
| CWG | 25 | 48 | 32 | 58.3499 | 0.42812 | −10.1570 | 0.18283 |
| CWG | 33 | 80 | 53 | 58.3481 | 0.42811 | −10.1571 | 0.18241 |
| CWG* | 49 | 96 | 63 | 58.3488 | 0.42811 | −10.1570 | 0.18241 |
| CWG | 65 | 128 | 84 | 58.3480 | 0.42812 | −10.1571 | 0.18241 |
| GJZ | 40 | 38 | 36 (20) | 58.2208 | 0.42808 | −10.1547 | 0.19198 |
| GJZ | 60 | 42 | 40 (28) | 58.2955 | 0.42813 | −10.1560 | 0.19010 |
| GJZ | 100 | 42 | 40 (28) | 58.3348 | 0.42816 | −10.1558 | 0.18289 |
| TMH | 40 | | 36 | 58.5874 | 0.4271 | −10.0823 | 0.1228 |
| TMH | 100 | | 36 | 58.4028 | 0.4279 | −10.1421 | 0.1670 |
| TMH | 100*e* | | 36 | 58.5471 | 0.4281 | −10.1585 | 0.1560 |

[a] Notation: *e*, equidistant radial grid; $m_{max}$ given in parentheses after $\ell_{max}$ when different.

resolution. Also the contributions by ACD (diamonds), GJZ (squares) and TMH (crosses) with radial finite differencing converge satisfactorily towards the same values at high $R$. For the finite difference methods the radial resolution has been found to be critical, and in fact the angular resolution has been kept constant or varied little in these calculations. ACD and GJZ report that results for a uniform radial grid (not shown in this paper) are much worse than for the non-uniform grids used here. The comparison supplied by TMH for $N_r = 100$ confirms this for $E_{kin}$ and $\omega$, although the differences are rather moderate. A non-uniform grid provides better resolution in the boundary layers, and even though the Ekman layer is not very thin at the moderate value of the Ekman number, good resolution of this layer seems to be essential.

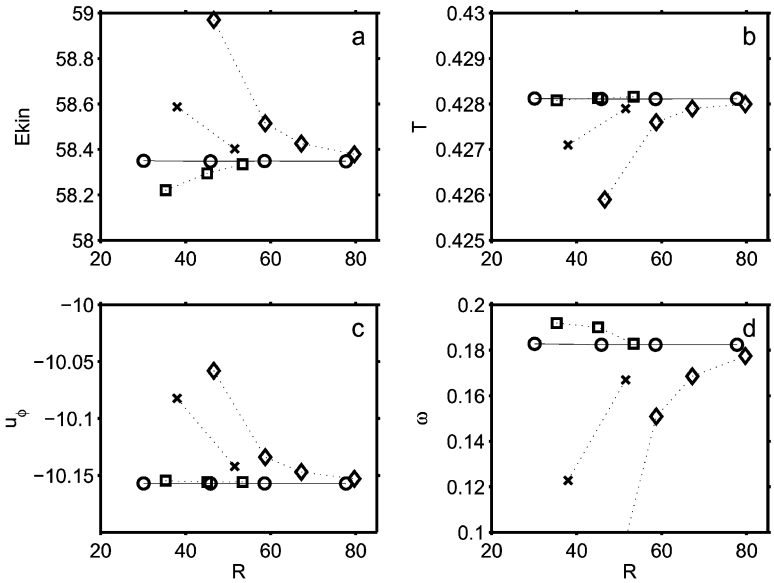


Fig. 2. Convergence of results for case 0: diamonds, ACD; circles, CWG; squares, GJZ; crosses, TMH. (a) Kinetic energy, (b) local temperature, (c) local azimuthal velocity, (d) drift frequency.

Table 2
Results for benchmark case 1[a]

| Group | $N_r$ | $N_\theta$ | $\ell_{max}$ | $E_{kin}$ | $E_{mag}$ | $T$ | $u_\phi$ | $B_\theta$ | $\omega$ |
|---|---|---|---|---|---|---|---|---|---|
| ACD | 48 | 46 | 44 | 29.965 | 601.912 | 0.3730 | −7.864 | −4.779 | −3.038 |
| ACD | 90 | 46 | 44 | 30.637 | 623.204 | 0.3729 | −7.669 | −4.912 | −3.102 |
| ACD | 150 | 46 | 44 | 30.732 | 625.681 | 0.3730 | −7.634 | −4.929 | −3.105 |
| ACD | 200 | 92 | 44 | 30.758 | 626.284 | 0.3730 | −7.626 | −4.933 | −3.105 |
| CWG | 21 | 40 | 26 | 30.5015 | 616.085 | 0.36281 | −7.2228 | −4.8456 | −3.0926 |
| CWG | 25 | 48 | 32 | 30.7214 | 626.572 | 0.37373 | −7.5941 | −4.9023 | −3.0852 |
| CWG | 33 | 64 | 42 | 30.7686 | 626.420 | 0.37390 | −7.6427 | −4.9358 | −3.1011 |
| CWG | 33 | 80 | 53 | 30.7714 | 626.406 | 0.37325 | −7.6211 | −4.9285 | −3.1016 |
| CWG | 41 | 96 | 64 | 30.7715 | 626.416 | 0.37337 | −7.6250 | −4.9288 | −3.1016 |
| CWG* | 49 | 96 | 63 | 30.7716 | 626.413 | 0.37337 | −7.6255 | −4.9284 | −3.1016 |
| CWG | 65 | 128 | 85 | 30.7734 | 626.409 | 0.37338 | −7.6250 | −4.9289 | −3.1017 |
| GJZ | 40 | 38 | 36 (20) | 30.1263 | 617.462 | 0.36226 | −7.0899 | −4.8972 | −2.992 |
| GJZ | 40 | 52 | 50 (44) | 30.5724 | 622.558 | 0.37314 | −7.6201 | −4.9101 | −3.083 |
| GJZ | 80 | 52 | 50 (44) | 30.7541 | 625.656 | 0.37325 | −7.6203 | −4.9301 | −3.100 |
| GJZ | 100 | 54 | 52 (52) | 30.7605 | 626.020 | 0.37336 | −7.6308 | −4.9232 | −3.101 |
| GJZ | 150 | 78 | 50 (44) | 30.7677 | 626.282 | 0.37328 | −7.6210 | −4.9333 | −3.101 |
| KS | 48 | 64 | 42 | 30.7709 | 626.434 | 0.37376 | −7.6376 | −4.9333 | −3.1009 |
| TG | 33 | 64 | 42 | 30.7695 | 626.402 | 0.37378 | −7.6387 | −4.9340 | −3.0997 |
| TMH | 70*e* | | 26 | 31.0298 | 623.092 | 0.3679 | −7.3525 | −4.9220 | −3.0949 |
| TMH | 70 | | 26 | 30.7901 | 627.607 | 0.3675 | −7.3330 | −4.9190 | −3.0735 |

[a] Notation: *e*, equidistant radial grid; $m_{max}$ in parentheses after $\ell_{max}$ when different.

### 6.2. Dynamo with insulating inner core (case 1)

Results for case 1 are listed in Table 2 and some of them are plotted against resolution in Fig. 3. Again the agreement among the various contributions is very satisfactory; the range covered in each of the diagrams is only 1% of the total value. The general agreement is particularly good between the three codes using

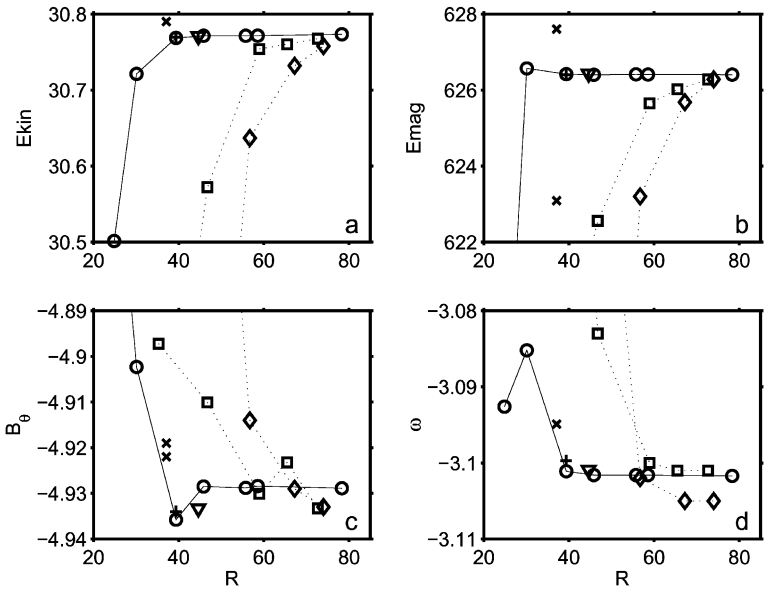


Fig. 3. Convergence of results for case 1: diamonds, ACD; circles, CWG; squares, GJZ; plus sign, TG; triangle, KS; crosses, TMH (uniform and non-uniform radial grid). (a) Kinetic energy, (b) magnetic energy, (c) local magnetic field component, (d) drift frequency.

Table 3
Results for benchmark case 2

| Group | $N_r$ | $N_r^{ic}$ | $N_\theta$ | $\ell_{max}$ | $E_{kin}$ | $E_{mag}$ | $E_{mag}^{ic}$ | $\omega$ | $\omega_{ic}$ | $\Gamma_L$ |
|---|---|---|---|---|---|---|---|---|---|---|
| ACD | 90 | 25 | 46 | 44 | 42.311 | 844.400 | 822.522 | −3.834 | −2.521 | −91.023 |
| ACD | 150 | 40 | 46 | 44 | 42.392 | 845.400 | 821.855 | −3.821 | −2.598 | −91.910 |
| ACD | 200 | 60 | 46 | 44 | 42.405 | 845.604 | 821.833 | −3.816 | −2.619 | −92.212 |
| ACD | 250 | 70 | 46 | 44 | 42.409 | 845.694 | 821.885 | −3.815 | −2.630 | −92.381 |
| CWG | 33 | 16 | 48 | 32 | 42.3295 | 849.003 | 824.255 | −3.7584 | −2.7393 | −94.407 |
| CWG | 49 | 16 | 64 | 41 | 42.3713 | 845.932 | 823.162 | −3.7984 | −2.6706 | −93.105 |
| CWG | 49 | 16 | 96 | 63 | 42.3882 | 845.605 | 822.667 | −3.8027 | −2.6594 | −92.979 |
| CWG* | 49 | 16 | 96 | 63 | 42.3878 | 845.604 | 822.672 | −3.8027 | −2.6593 | −92.978 |
| CWG | 49 | 20 | 96 | 63 | 42.3888 | 845.602 | 822.649 | −3.8027 | −2.6593 | −92.978 |
| CWG | 49 | 16 | 128 | 84 | 42.3881 | 845.606 | 822.673 | −3.8027 | −2.6595 | −92.979 |

Chebyshev expansion (circles, triangle and plus sign in Fig. 3), which is not surprising given that the codes are based on the same principles. For this method, only CWG (circles) provide results at variable resolution, but two codes with radial finite differencing seem to converge against the same values for the kinetic and magnetic energy, respectively. For the local values and the drift frequency convergence against a common point is less clear than for the energies, but the best resolved results agree within a quarter of a percent. For the local values the need to interpolate the respective fields between grid points is an additional source of error, which might explain the less systematic convergence behaviour.

CWG studied the influence of changing the time-step for two different spatial grids. Reducing the step by a factor of two lead to differences in the sixth decimal place. Therefore, a time-step which is smaller than what stability requires does not improve the solution significantly, at least in the weakly time-dependent regime of the benchmark dynamo.

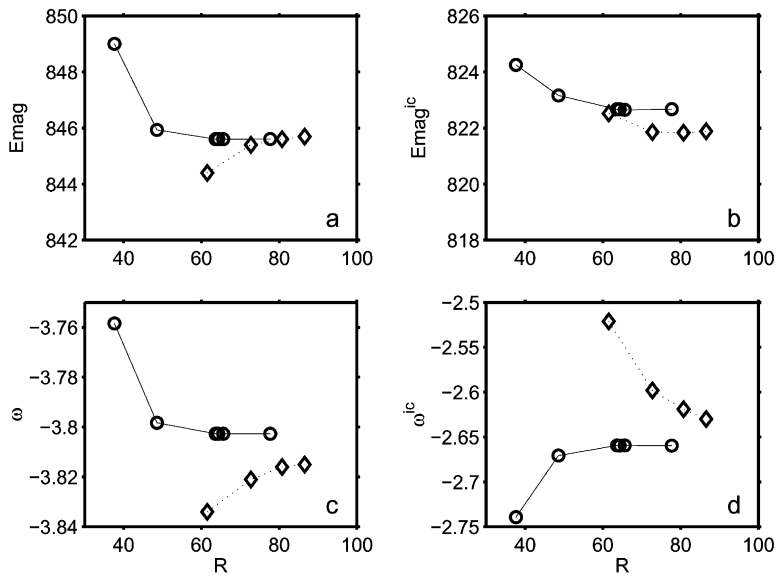


Fig. 4. Convergence of results for case 2: diamonds, ACD; circles, CWG. (a) Magnetic energy density in fluid shell, (b) magnetic energy density in inner core, (c) drift frequency, (d) rotation frequency of inner core.

### *6.3. Dynamo with conducting and rotating inner core (case 2)*

Results for case 2 have only been reported by two contributors. The validity of the results is somewhat reinforced by the use of two different code versions by CWG (labelled with and without an asterisk). The basis for both versions is the fully spectral dynamo code by Glatzmaier (1984), but the additions for treating a conducting and rotating inner core have been implemented independently and overall the codes differ in some details. The two solutions agree within better than $4 \times 10^{-5}$ for all requested properties. The results by ACD, who use a finite difference method in the radial direction, are in reasonable agreement with those by CWG (Table 3 and Fig. 4). The deviation is largest for the inner core rotation rate, about 1% at the highest resolution, but a quadratic extrapolation of ACD's results suggest that they converge against those by CWG.

The sum of the viscous and magnetic torques on the solid inner core is obviously zero because its rotation rate is steady. The viscous torque is positive (prograde) while the magnetic torque is negative (Table 3). GAG reports that the viscous torque on the stationary inner core of case 1 is also positive and cancels the negative viscous torque on the outer boundary so that the net torque on the fluid shell still vanishes, as it has to in steady state. It is interesting that the signs of the viscous torques on the two boundaries in the non-magnetic case 0 are opposite to what they are in case 1 and that the sign of the drift frequency $\omega$ differs between cases 0 and 1.

## 7. Discussion and conclusions

The comparison of codes that use finite differences in the radial direction with fully spectral methods suggests that the latter are more advantageous when high accuracy is required. In case of the partial finite difference methods, the radial resolution is clearly the accuracy-limiting factor. The exponential convergence behaviour of fully spectral methods is very helpful to pin down the solution to several significant digits, which is one aim of the benchmark study. Furthermore, an asset of the Chebyshev representation is that it allows one to calculate radial derivatives of the dependent variables on grid points with great accuracy. Because most computer time is used for the transformation in the angular coordinates, the additional time required for the Chebyshev transforms is far outweighed by the smaller number of radial grid levels that is needed to achieve a given accuracy. However, one must also keep in mind that the benchmark cases are simple in the sense that the spatial spectra drop off rapidly with wavenumber and time-dependence is weak, which makes them ideally suited for spectral methods. For chaotic dynamos at higher Rayleigh numbers and lower Ekman numbers, which require much higher spatial resolution, the spectral method becomes very expensive and may be less suited than other techniques for massively parallel computers. Unfortunately, a comparison study at such parameters would be far more difficult.

The overall level of agreement between different methods is remarkable when the resolution is sufficiently high. This allows us to define with great confidence a standard solution within narrow error

Table 4
Suggested standard solution with uncertainties

| | Case 0 | Case 1 | Case 2 |
|---|---|---|---|
| $E_{\rm kin}$ | $58.348 \pm 0.050$ | $30.733 \pm 0.020$ | $42.388 \pm 0.050$ |
| $E_{\rm mag}$ | | $626.41 \pm 0.40$ | $845.60 \pm 0.40$ |
| $E^{\rm ic}_{\rm mag}$ | | | $822.67 \pm 1.60$ |
| $T$ | $0.42812 \pm 0.00012$ | $0.37338 \pm 0.00040$ | |
| $u_\phi$ | $-10.1571 \pm 0.0020$ | $-7.6250 \pm 0.0060$ | |
| $B_\theta$ | | $-4.9289 \pm 0.0060$ | |
| $\omega$ | $0.1824 \pm 0.0050$ | $-3.1017 \pm 0.0040$ | $-3.8027 \pm 0.0250$ |
| $\omega_{\rm ic}$ | | | $-2.6595 \pm 0.0600$ |
| $\Gamma_{\rm L}$ | | | $-92.979 \pm 1.200$ |

limits for cases 0 and 1. We suggest that the best result from CWG be considered the standard. To estimate the range of uncertainty we require that the best-resolved results of two more codes (those by ACD and GJZ) fall into this range (Table 4). Because of the slower convergence of the latter two codes, the exact solution may be much closer to the suggested value than what the quoted accuracy suggests.

With only two completely independent contributions to case 2 we cannot claim the same level of confidence as in the other cases, but the convergence of the CWG results and the satisfactory agreement with the ACD solution justifies the selection of the best resolved result by CWG as a standard also in this case. Here, the uncertainty has been fixed to twice the difference between the best results by CWG and ACD, but not less than the uncertainty determined in case 1 for the same property (where applicable).

## References

Busse, F.H., Grote, E., Tilgner, A., 1998. On convection driven dynamos in rotating spherical shells. Stud. Geophys. et Geod. 42, 1–6.

Canuto, C., Hussani, M.Y., Quateroni, A., Zhang, T.A., 1987. Spectral Methods in Fluid Dynamics. Springer, Berlin.

Christensen, U., Olson, P., Glatzmaier, G.A., 1998. A dynamo model interpretation of geomagnetic field structures. Geophys. Res. Lett. 25, 1565–1568.

Christensen, U., Olson, P., Glatzmaier, G.A., 1999. Numerical modelling of the geodynamo: a systematic parameter study. Geophys. J. Int. 138, 393–409.

Dormy, E., Cardin, P., Jault, D., 1998. MHD flow in a slightly differentially rotating spherical shell, with conducting inner core, in a dipolar magnetic field. Earth Planet. Sci. Lett. 160, 15–30.

Glatzmaier, G.A., 1984. Numerical simulations of stellar convective dynamos. I. The model and method. J. Comput. Phys. 55, 461–484.

Glatzmaier, G.A., Roberts, P.H., 1995. A three-dimensional convective dynamo solution with rotating and finitely conducting inner core and mantle. Phys. Earth Planet. Inter. 91, 63–75.

Grote, E., Busse, F.H., Tilgner, A., 2000. Regular and chaotic spherical dynamos. Phys. Earth Planet. Inter. 117, 259–272.

Kageyama, A., Sato, T., 1995. The complexity simulation group, computer simulation of a magnetohydrodynamic dynamo. Phys. Plasma 2, 1421–1431.

Katayama, J.S., Matsushima, M., Honkura, Y., 1999. Some characteristics of magnetic field behavior in a model of MHD dynamo thermally driven in a rotating spherical shell. Phys. Earth Planet. Inter. 111, 141–159.

Kuang, W., Bloxham, J., 1997. An Earth-like numerical dynamo model. Nature 389, 371–374.

Sakuraba, A., Kono, M., 1999. Effect of the inner core on the numerical solution of the magnetohydrodynamic dynamo. Phys. Earth Planet. Inter. 111, 105–121.

Tilgner, A., 1999. Spectral methods for the simulation of incompressible flow in spherical shells. Int. J. Num. Meth. Fluids 30, 713–724.